Annals of Biomedical Engineering, Vol. 42, No. 9, September 2014 (© 2014) pp. 1989–2001
DOI: 10.1007/s10439-014-1051-3

Simulation of Self Expanding Transcatheter Aortic Valve in a Realistic Aortic Root: Implications of Deployment Geometry on Leaflet Deformation

PAUL S. GUNNING, TED J. VAUGHAN, and LAOISE M. MCNAMARA

Biomechanics Research Centre (BMEC), Department of Biomedical Engineering, National University of Ireland Galway, Galway, Ireland

(*Received 16 January 2014; accepted 30 May 2014; published online 10 June 2014*)

Associate Editor Estefanía Peña oversaw the review of this article.

Abstract—Self expanding Transcatheter Aortic Valve Replacements (TAVR) can conform to the geometry of the aortic annulus and the calcified leaflet complex, which may result in leaflet distortion and altered leaflet kinematics, but such changes have not yet been characterized. In this study we developed a computational model to investigate the deployment of a self expanding TAVR in a realistic aortic root model derived from multi-slice computed tomography (MSCT) images. We simulated TAVR crimping/deployment in realistic and idealized aortic root models, followed by diastolic loading of the TAVR leaflets in its final deployed configuration. The TAVR deployed in a realistic aortic root had increased peak loading in the commissural region of the leaflets compared to TAVRs under idealized circular deployment conditions (2.97 vs. 1.52 MPa). Furthermore, orientation of the TAVR in the asymmetric aortic annulus such that the commissures of the TAVR are aligned with the native valve commissures minimized the effect of TAVR stent distortion on peak stresses in the TAVR leaflets (2.97 vs. 2.35 MPa). We propose that preoperative planning of the orientation of the TAVR in the aortic root annulus might minimize the impact of potential stent distortion on leaflet function and may in turn increase long term leaflet durability.

Keywords—Transcatheter aortic valve, Finite element analysis, Self expanding, Patient-specific.

INTRODUCTION

The aortic valve is a blood flow control device, which is responsible for maintaining the unidirectional flow of blood during the cardiac cycle.[24] Aortic stenosis (AS) is an age related degenerative disease of the aortic valve that causes progressive narrowing of the valve and aortic regurgitation.[19] Conventional open heart surgery to implant surgical mechanical or bioprosthetic valves to replace the stenotic valve is the current gold standard of care for the treatment of severe AS.[19] However approximately 30% of patients presenting with symptomatic AS are refused this highly invasive surgery because of high preoperative mortality rates in patients, particularly patients of advanced age or those with pre-existing illnesses.[11,19] Transcatheter Aortic Valve Replacement (TAVR) is a percutaneous alternative to open heart surgery allowing for the treatment of this cohort of high-risk patients for which conventional surgery is deemed inappropriate.[16,19,27] TAVRs consist of animal derived tissue leaflets, which are mounted onto an expandable metallic frame and are delivered to the site of the native stenotic valve in a crimped configuration *via* a catheter through a transfemoral or transapical based approach. Once positioned correctly the valve stent is expanded radially, using a balloon or by means of self expanding stent material and this expansion pushes the stenosed valve against the aortic annulus and sinus walls.

Calcium deposits, varying in both size and density, are present within the native aortic valve.[19,29] While conventional open-heart surgical techniques can account for these deposits and ensure optimal circular implantation of surgical valves, deployment of TAVRs against these deposits can result in non-concentric deployment of the valve stent, which can lead to altered leaflet kinematics.[19,26] The final deployment morphology of a TAVR stent is dependent on the interaction between the valve stent and the aortic root.[19,33] Currently, there are two TAVR stent materials used, balloon

Address correspondence to Laoise M. McNamara, Biomechanics Research Centre (BMEC), Department of Biomedical Engineering, National University of Ireland Galway, Galway, Ireland. Electronic mail: Laoise.McNamara@nuigalway.ie

expandable stainless steel/cobalt chromium and self expanding Nitinol. Balloon expandable stainless steel/cobalt chromium stents force the asymmetric annulus to conform to the circular geometry of the stent ensuring optimal circular implantation and leaflet kinematics.[19] In contrast, self expanding stents rely on the superelastic property of Nitinol, rather than balloon inflation, for stent deployment. The lower hoop strength allows for improved stent apposition to the calcified aortic root and can minimize the occurrence of paravalvular leakage. However the conformance of the Nitinol stent to the calcified leaflets/asymmetric annulus can exacerbate valve distortion and may lead to irregular leaflet kinematics.[19,26]

Computational approaches have been used previously to analyze TAVRs, investigating distorted leaflet geometries, valve positioning, migration forces, and the biomechanical interaction of the valve stent with the aortic root.[2,6,29,34] It has been shown that highly eccentric leaflet geometries show a 143% increase in peak leaflet stresses compared to circular geometries, as well as being more susceptible to intravalvular leakage.[29] However this study focused on idealized eccentric leaflet geometries alone and did not explicitly model a TAVR stent and as such did not incorporate the complex interaction between the TAVR stent and the native anatomy. Recent studies have investigated balloon expandable TAVRs in patient-specific computational models[2,34] but the deployment morphology of Nitinol TAVR stents in patient-specific anatomy and the resultant effect of leaflet deformation have yet to be investigated. With a number of current generation TAVRs (Lotus Valve (Sadra Medical, Boston Scientific), Aortx (Hansen Medical), CoreValve and Engager Valve (Medtronic) and Portico Valve (St. Jude Medical)) using self expanding stent technologies,[19] further patient-specific numerical modeling is warranted to investigate the effect of aortic root morphologies on self expanding stent deployment geometries.

The objective of this research is to develop a patient-specific model of the deployment of a self expanding Nitinol TAVR and apply this model to investigate the effects of deployment geometry on leaflet deformation and stress distribution. Specifically, we simulate TAVR crimping and deployment into a realistic patient-specific aortic root model and compare leaflet stresses and closing kinematics to TAVRs deployed in idealized orifices.

MATERIALS AND METHODS

Transcatheter Aortic Valve Model

A self expanding Nitinol TAVR was modeled in this study, consisting of a self expanding valve stent, a paravalvular skirt and pericardial tissue leaflets. The valve stent was a diamond shaped, repeating unit close cell design consisting of 2 rows of 15 cells orientated around the circumference of the frame (Fig. 1a). The finite element model was generated in Abaqus 6.12 (SIMULIA, Providence, RI) by meshing a planar frame model and then wrapping this mesh into a cylinder by converting nodal coordinates from a Cartesian coordinate system into a cylindrical coordinate system; see Fig. 2b. The cylindrical shell mesh was then extruded, giving the valve stent a 0.25 mm thickness. The stent struts were meshed with C3D8R elements, with four elements through the strut thickness and seven elements in the width dimension, following best practices for stent analysis within Abaqus. Enhanced hourglass control was used to avoid the excessive flexibility of the reduced integration first order elements. A paravalvular skirt was attached to the TAVR stent to mitigate paravalvular leakage and for leaflet/stent attachment. A rigid tie constraint was used to model the interaction between the skirt and the cells of the TAVR stent. Tissue leaflets were initially arranged in a planar configuration and using displacement controlled finite element simulation, leaflet coaptated geometries were formed as described further in "Boundary and Loading Conditions: Simulation Steps" section (Fig. 1c). TAVR leaflets were meshed with eight noded linear brick elements with enhanced hourglass control (C3D8R) with three elements through the leaflet thickness.

Aortic Root Models

In this study we develop finite element models of the crimping, deployment and diastolic loading of a TAVR in an aortic root model. The TAVR was deployed into a realistic patient-specific aortic root model and compared with TAVR deployment in idealized circular and elliptical models, similar to those modeled in Sun *et al.*[29]

Patient-Specific Aortic Root Geometry

Multi-slice computed tomography (MSCT) images were taken of a stenosed aortic root at peak diastole of a 89 year old pre-TAVR patient (slice thickness = 0.625 mm, slice dimensions = 512 × 512 and pixel spacing = 0.5 mm), see Fig. 2a. Leaflet calcifications were present on the aortic leaflets, extending from the basal attachments up to the leaflet commissures. MSCT images were imported into Mimics 14.1 Imaging Software (Materialise, Leuven, Belgium). A 3D anatomically accurate model of the aortic root was created by manually thresholding between Hounsfield units of −50 to 700, which were chosen to most

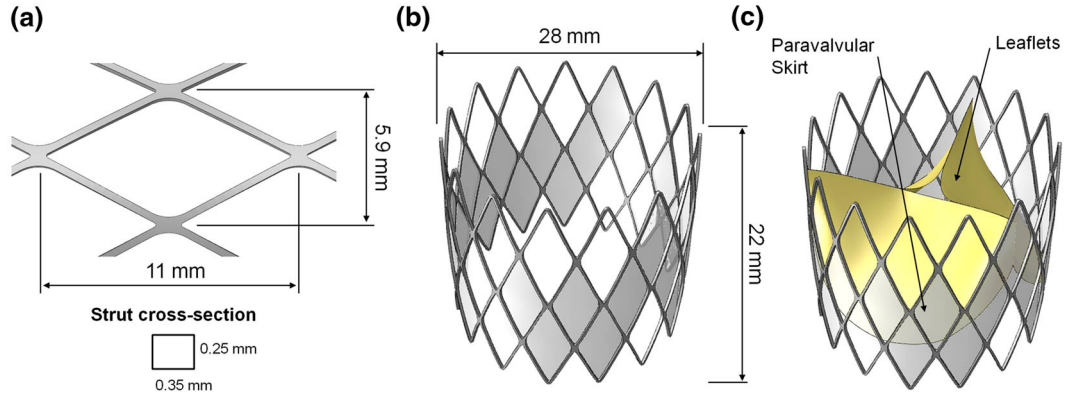

FIGURE 1. Unit cell geometry (a), TAVR stent geometry (b) and final TAVR design used in the simulations (c).

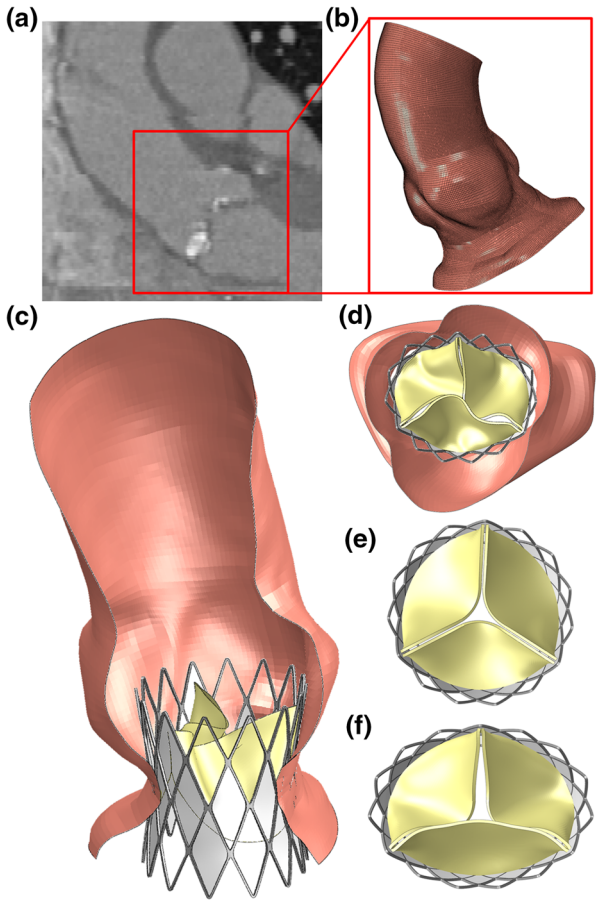

FIGURE 2. CT Image of aortic root (a) and reconstructed mesh geometry (b). Views of TAVR stent geometry deployed in realistic aortic root geometry (c) and (d) and idealized circular and eccentric geometries (e) and (f).

accurately preserve the aortic root geometry. Segmentation *via* thresholding allowed for the separation of the aortic root beginning at the left ventricular outflow tract (LVOT) to the sinotubular junction from the surrounding atria and ventricles. Coronary ostia's and calcified aortic valve leaflets were omitted to simplify the model geometry. This geometry was imported as an STL model into Abaqus 6.12 (SIMULIA, Providence, RI) and discretised into a quadrilateral mesh and assigned shell elements (S4) of 2 mm thickness, similar to previous approaches,[6,28] for finite element analysis (Fig. 2b). Dimensions of the aortic annulus was defined as the maximum (D_{max}) and minimal (D_{min}) diameter measurements of the basal ring below the aortic valve cusps. For the aortic root model chosen, D_{max} and D_{min} were 28.4 mm and 17.6 mm respectively, giving an approximated eccentricity of 0.78 using Eq. (1). Figures 2c and 2d show final TAVR deployment in the realistic aortic root model.

Idealized Aortic Root Geometries

In order to obtain idealized TAVR stent geometries, TAVR stents were crimped and deployed into idealized circular and eccentric aortic root geometries, as shown in Figs. 2e and 2f. Aortic root geometries were chosen such that, upon valve deployment, TAVRs were implanted in idealized circular and eccentric geometries (eccentricity = 0.68, D_{min} = 19.6 & D_{max} = 27.2) representing *in vivo* TAVR geometries obtained from MSCT images in patients with AS.[26,29] The eccentric TAVR geometry was generated by modifying the eccentricity of an ellipse according to Eq. (1):

$$e = \sqrt{1 - \left(\frac{b}{a}\right)^2} \tag{1}$$

where a and b are the lengths of the major and minor axes of an ellipse.[29] Idealized aortic root geometries were meshed using eight-noded linear reduced integration elements with enhanced hourglass control (C3D8R) in the finite element solver Abaqus 6.12.

Constitutive Models

The valve stent was assigned superelastic material properties using the Abaqus 6.12 user material sub-

routine (VUMAT) based upon the Auricchio and Taylor model.[3,4] The material parameters (Table 1) were derived from a previous study correlating the numerical model to an experimental crush test of a Nitinol TAVR stent.[33] An incompressible hyperelastic isotropic Mooney–Rivlin model was used to represent the mechanical behavior of the realistic aortic root. The model is defined using the following strain energy density function, U, as in Eq. (2):

$$U = C_{10}(\overline{I}_1 - 3) + C_{01}(\overline{I}_2 - 3) + \frac{1}{D}(J-1)^2 \qquad (2)$$

where C_{10} and C_{01} are material parameters with the dimensions of stress, D is the incompressibility parameter, which was assigned a value of $1e^{-6}$ assuming near incompressibility,[12] and I_1 and I_2 are the first and second invariant of the right Cauchy–Green deformation tensor C and are defined as follows:

$$\overline{I}_1 = trC, \qquad \overline{I}_2 = \frac{1}{2}\left[\overline{I}_1^2 - trC^2\right]$$

The following material constants were adopted: $C_{10} = 0.5516$ MPa and $C_{01} = 0.1379$ MPa.[1,8]

The incompressible hyperelastic isotropic Marlow model[17] was used to represent the mechanical behavior of the glutaraldehyde fixed pericardial leaflet tissue using the following strain energy potential, as in Eq. (3):

$$U = U_{\text{dev}}(\overline{I}_1) + U_{\text{vol}}(J_{\text{el}}) \qquad (3)$$

where U_{dev} is the deviatoric response of the tissue derived from experimental stress strain data in the circumferential direction obtained from biaxial testing of bovine pericardial tissue samples obtained from Li *et al.*[16] For both aortic root and TAVR leaflet models, near incompressibility was assumed and tissue densities of 1140 kg/m^3 were used.

TABLE 1. Material parameters for superelastic material model [33].

Parameter	Value
E_A (Austenite elasticity)	50,000 MPa
υ_A (Austenite Poisson's Ratio)	0.3
E_M (Martensite Elasticity)	25,000 MPa
υ_M (Martensite Poisson's Ratio)	0.3
σ_s^{AS} (Start of transformation loading)	380 MPa
σ_f^{AS} (End of transformation loading)	400 MPa
σ_s^{SA} (Start of transformation unloading)	250 MPa
σ_f^{SA} (End of transformation unloading)	220 MPa
ε_L (Strain limit)	7%
t_0 (Reference temperature)	37°C
Density	6,700 kg/m^3

Boundary and Loading Conditions: Simulation Steps

Step 1: Stent Deployment

Abaqus/Explicit finite element solver was used to model the TAVR crimping and deployment. Prior to valve stent deployment, the valve stent diameter was reduced from 28 to 10 mm using a rigid cylindrical surface. Radial displacement boundary conditions were placed on the rigid surface, reducing the surface diameter and thus crimping the stent; see Fig. 3 (Step 1). A local cylindrical coordinate system was defined and two sets of nodes oriented at 180° to each other were constrained in the tangential and axial directions see Fig. 3 (Step 1). Penalty enforced surface-to-surface based contact with zero contact friction was defined between the crimp surface and the stent outer diameter, wherein the crimp surface was assigned as the master surface. The paravalvular skirt had a much lower stiffness than the Nitinol TAVR stent and was not included in this step as it was deemed to have a negligible impact on the overall mechanical behavior of the stent.[13] The paravalvular stent was introduced into the analysis following stent deployment, whereby a cylindrical surface was generated which covered the diamond cells of the deployed stent geometry. In the realistic patient-specific model, the TAVR stent was deployed such that the TAVR was positioned at the annular level of the aortic root, with an equal distribution of the TAVR stent above and below the annulus. Contact with the aortic root wall was simulated by defining a penalty surface-based contact between the valve stent (master) and the aortic root wall (slave) using a coefficient of friction of 0.25. The aortic root was constrained at the vessel ends in the longitudinal and circumferential directions allowing radial displacements to occur only.

TAVR Orientation

TAVRs were orientated in the eccentric and realistic aortic annulus orifices in multiple configurations to investigate the impact of TAVR orientation on leaflet deformation and kinematics. In the first configuration, leaflets were orientated such that one of the lines of coaptation was aligned with the major axis of the ellipse (*Parallel*). In the second configuration, leaflets were orientated 90° such that the line of coaptation was perpendicular to the major axis of the ellipse (*Perpendicular*). TAVRs were orientated similarly in the approximated ellipse of the realistic aortic annulus model. In addition to this, the TAVR was also orientated in a third configuration such that the commissures of the TAVR were aligned with the existing commissures of the native valve (*Commissure Aligned*). As such six TAVRs models were created, one for

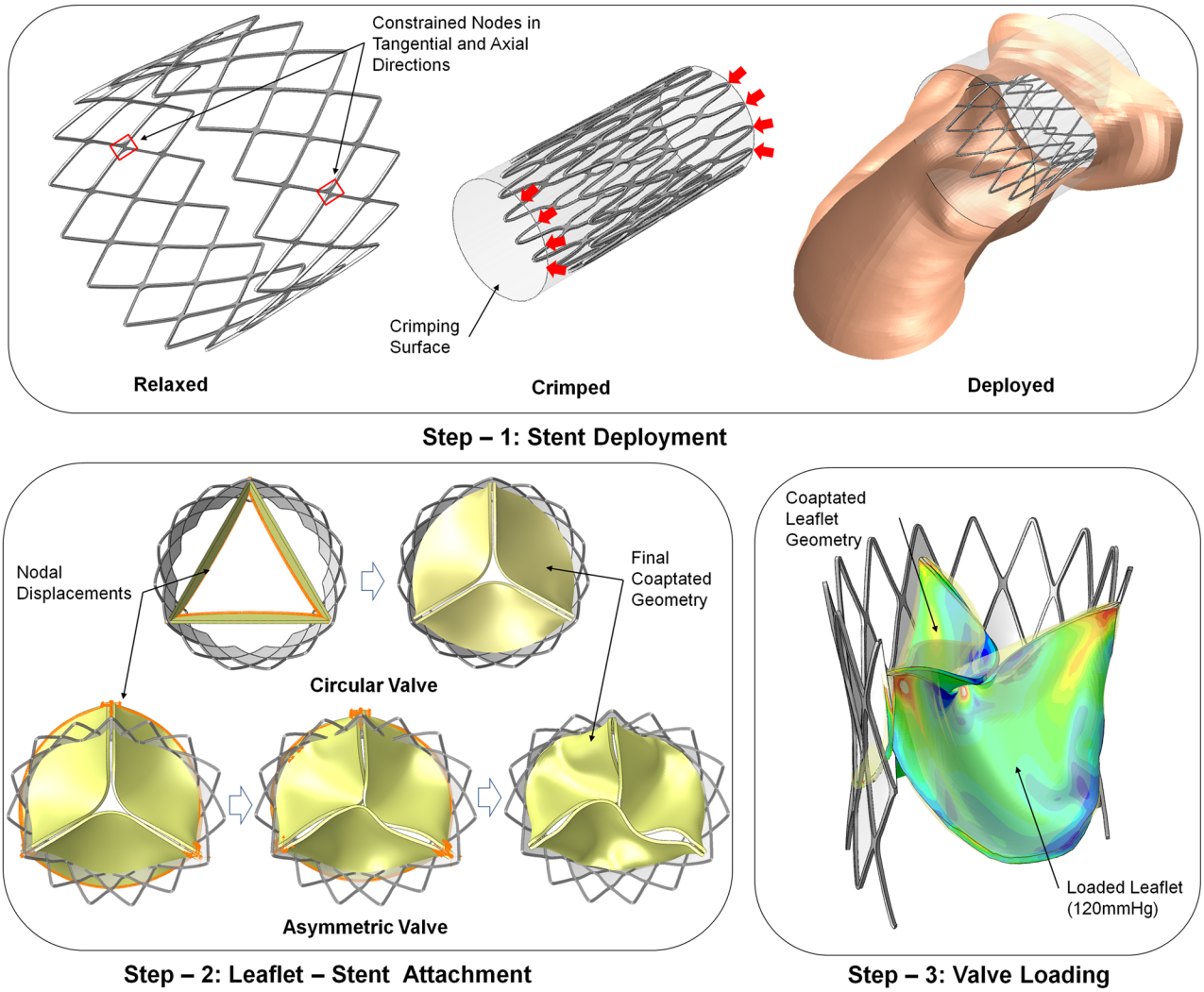

FIGURE 3. Steps involved in the simulation beginning with valve stent crimping and deployment (Step 1), leaflet attachment (Step 2) and valve loading (Step 3).

circular deployment, two for elliptical deployment (*Parallel and Perpendicular*) and a further three for realistic deployment (*Parallel, Perpendicular and Commissure Aligned*).

Step 2: Leaflet—Stent Attachment and Valve Loading

Leaflets were initially arranged in a planar state oriented at 60° to each other with leaflet commissures aligned with the commissures of the valve stent; see Fig. 3 (Step 2). Displacements were applied to nodes on the leaflet attachment edge translating leaflet nodes to their corresponding attachment point on a circular valve skirt and stent; see Fig. 3 (Step 2). A small pressure load was placed on the ventricular side of the leaflets to aid in leaflet bending to the attachment points. Following attachment, leaflets were assumed to be at zero transvalvular pressure and at the start of coaptation. For non-concentric valve deployments, the attached circular leaflet geometries were displaced to their new attachment points on the distorted stent geometries. Leaflet closure was simulated using Abaqus/Explicit solver using quasi-static procedures. A mass scaling strategy was chosen such that the ratio of kinetic energy to internal energy did not exceed 10%, ensuring inertial forces did not affect the solution.

Leaflet closure was simulated with a peak diastolic pressure gradient of 120 mmHg applied uniformly to the aortic side of the leaflets[16,18,29] based on experimental measurements from native and bioprosthetic valves under normotensive pressure conditions[9,25] and similar to previous computational simulations of bioprosthetic valves.[16,18,29] Leaflet contact was simulated using the penalty contact method using three master/slave pairs and a coefficient of friction of 0.1.[16,18,29] To avoid unrealistic contact chattering at initial leaflet

impact during valve closure, a mass proportional Rayleigh damping coefficient was used. Damping also simulated the viscous force dissipation created at the leaflet surface during movement through the blood. As mass damping may lead to artificial stiffening behavior of the leaflet, damping was introduced to the model *via* an arbitrarily soft thin skin layer (Elastic Modulus = 1000 Pa, Poisson's Ratio = 0.3, Density = 1100 kg/m^3 and a thickness of 0.0386) on the ventricular side of each leaflet.[12] As nodes were shared between the skin layer and the underlying leaflet mesh, no relative motion between the two layers was possible. For the purpose of this simulation, dynamic motion of the aortic root was not incorporated, as the focus of this research is the effect of asymmetric deployment on leaflet strain distribution at peak diastole. As such the TAVR stent was considered static during diastolic loading of the valve. Simulations were performed using Abaqus Explicit 6.12 with a typical solver time of 24 h using 12 compute nodes of a SGI Altix ICE 8200EX cluster with each compute node having two Intel Xeon E5650 hex-core processors and 24 GB of RAM.

RESULTS

Deployed TAVR Geometries and Aortic Root Stress Distribution

Figures 2c, 2d, 2e, and 2f show the deployment geometries of the realistic and idealized, circular and elliptical deployed TAVR stent geometries. In the idealized deployment geometries, the cross sectional profile of the stent remained constant throughout the axial length of the stent. Qualitatively it can be seen that the leaflets in the circular configuration had well defined coaptation lines with each coaptation line also being an axis of symmetry (Fig. 4a). Coaptated leaflet geometries in the eccentric configuration were also symmetrical however had only one axis of symmetry existing along the minor/major axis of the ellipse depending on leaflet orientation (Figs. 4b and 4c). In the realistic TAVR deployment, the TAVR stent was deployed such that an equal portion of the stent extended above and below the annulus region. This resulted in the stent being more constrained by the aortic annulus than at the proximal and distal regions of the stent protruding into the LVOT and sinus regions respectively (see Fig. 2c). The TAVR stent deployed in the realistic model showed an irregular asymmetric geometry with an approximated final deployed eccentricity of 0.65 measured at the mid section of the stent constrained by the aortic annulus, as shown in Fig. 2c. Deployment into a completely asymmetric orifice lead to highly disorganized coaptation lines and distorted leaflets with no lines of symmetry present, as shown in Figs. 4d, 4e, and 4f. The highly disorganized leaflet coaptation lines lead to the free edge of one or more leaflets contacting the belly of the opposing leaflet(s), causing a pivot point for the opposing leaflet to bend over, as shown in Figs. 5 and 6. Figure 7a shows the von Mises stress distribution in the aortic root as a result of TAVR expansion. Highest stress concentrations (0.24 MPa) were found at the aortic annulus level and were observed at the contact interface between the stent strut and the aortic wall adjacent with the minor axis of the ellipse. As the self expanding stent provides equal radial force in all directions, orientation of the valve did not change stress distribution results. Figure 7b shows the von Mises stress distribution in the self expanding TAVR stent following deployment. Peak stresses of 399 MPa were recorded in the struts in the vicinity of cell junctions at the centre of the valve stent.

Leaflet Stress Distribution for Idealized Leaflet Configurations

The finite element contour plots of Max Principal Stress for the idealized circular and eccentric configurations under peak diastolic loading are shown in Figs. 4a, 4b, and 4c. In the *circular* deployed valve, a relatively homogenous distribution of leaflet Max Principal Stress was observed across the leaflet, with peak values occurring at the leaflet commissures; see Fig. 4a. Average peak stress at each leaflet commissure was 1.52 MPa with a low standard deviation (0.02) indicating minimal variance between peak stresses in each leaflet. Peak stresses were found to vary in magnitude and in location in the distorted eccentric TAVR geometry. In the *eccentric-parallel* configuration, a maximum commissural stress of 3.3 MPa was recorded in the commissures of the leaflets with their coaptation line parallel with the major axis of the ellipse, as shown in Fig. 4b. In the *eccentric perpendicular* configuration, a further increase in peak commissural stress was recorded, with a peak stress of 3.55 MPa recorded in the commissures of the leaflet opposing the coaptation line parallel to the major axis of the ellipse, as indicated in Fig. 4c. Peak Maximum Principal Stresses recorded in each leaflet of all valve configurations are summarized in Table 2. As peak stress may be influenced by local edge effects caused by applied boundary conditions, we also analyzed the 99th percentile results with respect to leaflet volume, as shown in Fig. 8. For the idealized *circular, eccentric-parallel* and *eccentric-perpendicular* configurations, a similar proportion of the leaflets experienced stresses in the 0–0.2 MPa range (31.3%, 30.5%, and 29.1% respectively). For the *circular* and *eccentric-parallel* valves, a larger proportion

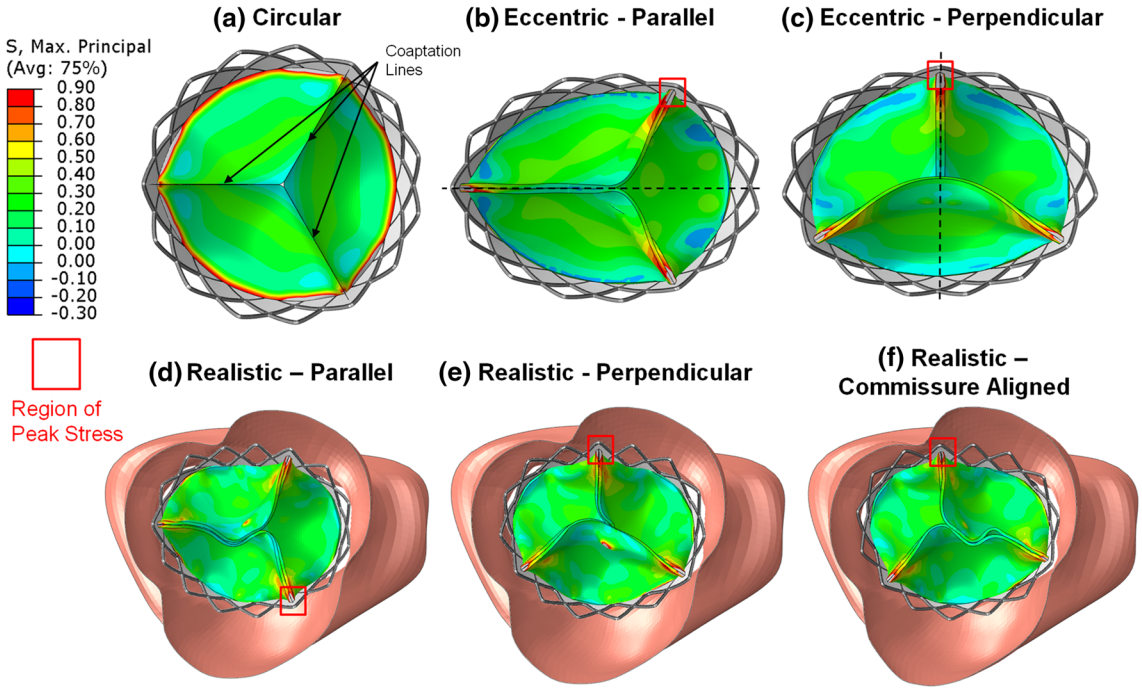

FIGURE 4. 99th percentile Maximum Principal Stress in TAVR Leaflets under idealized deployment conditions: (a) circular, (b) eccentric-parallel and (c) eccentric-perpendicular and under realistic deployment conditions in (d) realistic-parallel, (e) realistic-perpendicular and (f) realistic commissure aligned orientations. Red boxes indicate regions of peak stress.

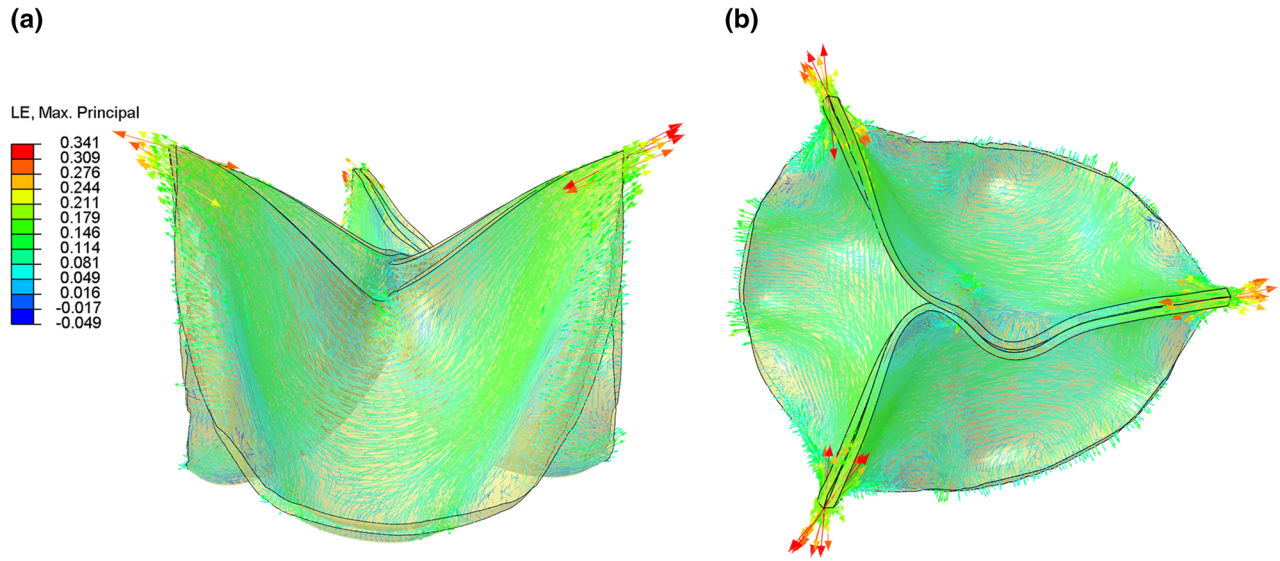

FIGURE 5. Transverse and axial views of the vector plot of Maximum Principal Stress at peak loading showing circumferential alignment of strains in the commissure regions of each leaflet.

of the leaflet volumes were stressed in the 0.2–0.4 MPa range (53.5% and 54% respectively), compared to the *eccentric-perpendicular* valve (49.2%). A higher percentage volume of the tissue leaflet was stressed in the 0.4–0.6 MPa range for the *eccentric-perpendicular* configuration (16.4%) compared to the *circular* and *eccentric-parallel* models (10.7% and 11.6%). For all configurations, a small volume of leaflet tissue experienced stress levels >0.8 MPa (3.4–4.5%) (Fig. 8).

Leaflet Stress Distribution for Realistic Leaflet Configuration

TAVRs deployed in the realistic aortic root anatomy showed an increase in peak Maximum Principal

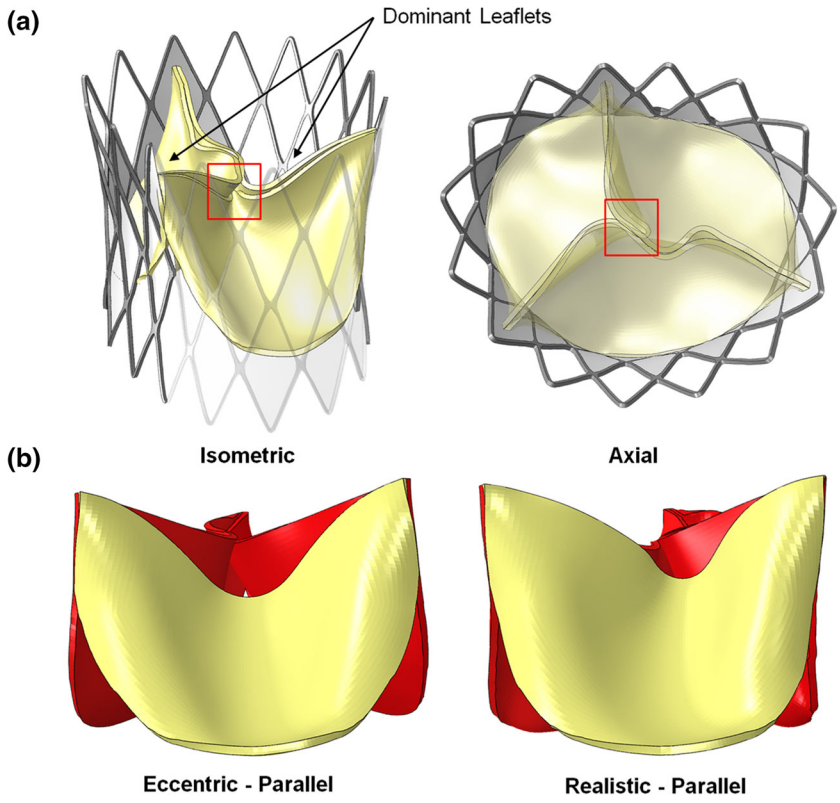

FIGURE 6. Isometric and axial views of leaflet coaptation mismatch (highlighted in red box) in a TAVR stent deployed in a realistic aortic root model, showing disorganized coaptation lines with dominant leaflets bending over the other leaflet during valve closure creating increased stresses in the commissures of the less dominant leaflet (a). Relative position of each leaflet position to each other (dominant leaflets in red) in the initial configuration following translation to distorted stent geometry in the parallel orientation of the eccentric (b) and realistic (c) deployed TAVRs.

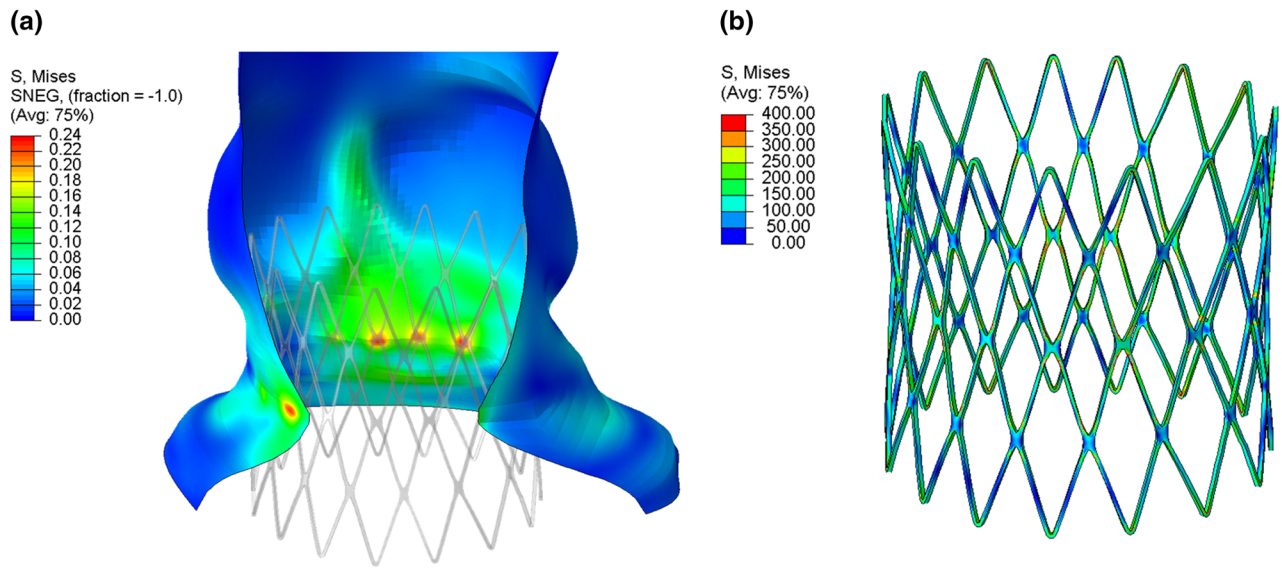

FIGURE 7. Von Mises stress distribution in the aortic root (a) and stent struts following stent deployment (b).

Stresses in each respective configuration compared to the idealized circular model, see Figs. 4d, 4e, and 4f. In the *realistic-parallel* configuration, a peak leaflet stress of 2.53 MPa was recorded in the leaflet opposing the coaptation line parallel to the major axis of the approximated ellipse (Fig. 4d). Orientating the valve

TABLE 2. Peak Maximum Principal Stresses recorded in each leaflet under different deployment configurations.

Valve configuration	Leaflet 1 (MPa)	Leaflet 2 (MPa)	Leaflet 3 (MPa)	STD
Circular	1.52	1.51	1.48	0.02
Eccentric-parallel	2.95	3.19	3.3	0.17
Eccentric-perpendicular	3.23	2.97	3.55	0.29
Realistic-parallel	1.97	2.53	2.09	0.29
Realistic-perpendicular	2.97	2.16	1.97	0.53
Realistic-commissure aligned	2.02	2.35	2.27	0.17

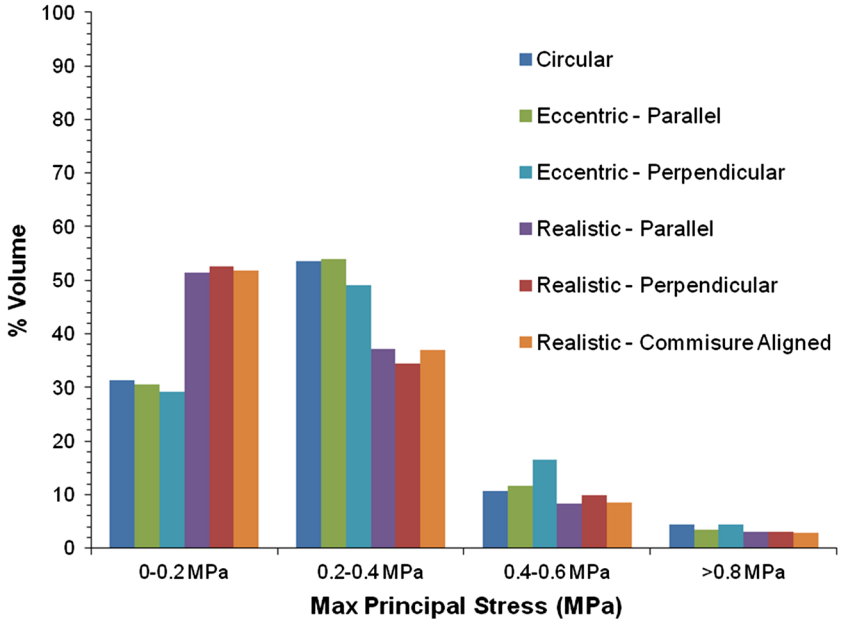

FIGURE 8. Max Principal Stress distribution as a function of percentage volume in each deployment configuration.

into the *realistic-perpendicular* configuration resulted in an increase in peak leaflet maximum principal stress to 2.97 MPa (Fig. 4e). In the *realistic commissure* aligned model, whereby commissures of the TAVR are aligned with the commissures of the native valve, peak stresses in the commissures were the lowest of the three orientations with a peak maximum principal stress value of 2.35 MPa.

A large proportion of the leaflet tissue volume in the realistically deployed valves experienced stresses in the 0–0.2 MPa range (51.5–52.5%), compared to an average of 30.3% in the idealized circular and eccentric models; see Fig 8. For the *realistic-parallel*, *perpendicular* and *commissure aligned* models respectively, 37.1%, 34.5%, and 37% of the tissue leaflet volumes had stress levels of 0.2–0.4 MPa, and these were lower than those reported for the idealized valve configurations (49.1–54%). A small volume of leaflet tissue was subjected to stress in the 0.4–0.6 MPa range for all realistic TAVR deployment configurations (8.4–9.9%), and these were lower than the maximum leaflet volume in the idealized models at this stress range (16.45%). For all configurations, a small volume of leaflet tissue experienced stress levels >0.8 MPa (2.9–3.1%).

DISCUSSION

In this study we developed finite element models of the deployment of a self expanding TAVR in a realistic patient-specific aortic root model at various orientations, and compared these to idealized deployment configurations to investigate the impact of distorted TAVR stent geometry on leaflet deformation and stress distribution. Our results show that TAVR deployment in a realistic aortic root lead to an irregular asymmetric stent morphology (approximated eccentricity = 0.65) and as a result the TAVR leaflets had highly irregular asymmetric leaflet coaptation geometries, compared to those of the idealized circular deployed TAVR. The tissue leaflets of the realistic TAVR had a more heterogeneous stress distribution than circularly deployed valves, with a higher proportion of the tissue leaflet volume experienced stresses

less than 0.2 MPa. The peak stresses within the leaflets of the TAVR deployed in the aortic root model were higher than peak stresses in leaflets when deployed in a circular configuration (2.97 vs. 1.52 MPa). Peak leaflet stresses (2.97 MPa) were highest when the TAVR was orientated in the perpendicular configuration with one line of leaflet coaptation orientated perpendicular to the major axis of the annulus. While orientating the TAVR in the parallel configuration lowered peak stresses further (2.53 MPa), it was found that orientating the TAVR such that its commissures were aligned with commissures of the native valve minimized average commissural peak stresses the most in the distorted stent geometry (2.35 MPa). The findings of this study show that distorted self expanding TAVR stent geometry can result in increases in leaflet peak stresses. Orientation of the TAVR to a commissure aligned position within the aortic annulus can minimize the effect of stent distortion on leaflet stress elevations.

The modeling of a complex mechanical environment of the *in vivo* aortic root with a self expanding TAVR stent necessitated a number of assumptions. The TAVR model used was a generic model, not directly based on any clinically used TAVR designs, but it was representative of the existing short profile Nitinol TAVR designs with scallop shaped leaflets such as the Boston Scientific Lotus TAVR, the JenaValve and Heart Leaflet Technology TAVR devices.[21] In reconstruction of the aortic root from CT data, the native leaflets were not included, due to the difficulties in identification and segmentation of the thin leaflets from the surrounding aortic root. As such our simulations do not incorporate the interaction between the calcified leaflets and the stent during valve deployment, which may exacerbate stent distortion and leaflet kinematics. Balloon aortic valvuloplasty can be used prior to TAVR deployment, to increase the prevalence of circular deployment by fracturing calcific nodules.[37] As leaflet calcifications were not incorporated in our model, this procedure was not simulated. In addition to this, the aortic annulus did not undergo dimensional changes in shape during the cardiac cycle as seen *in vivo*.[5] However as annulus reshaping is negligible, due to loss of tissue compliance associated with aging, calcific deposits, and the scaffolding effect caused by valve oversizing, a static model was deemed appropriate.[5,10]

Although anisotropic constitutive laws have been used to model aortic root and pericardial leaflet behavior,[2,16] representing the dominant alignment of fibers due to the natural organization of collagen in the aortic root and the effects of glutaraldehyde/pressure based fixation of pericardial tissue,[16,23] in our simulations we implemented isotropic constitutive laws fitted to the circumferential and stiffest directions of aortic root and pericardial tissue respectively. We deemed the use of isotropic hyperelastic material model appropriate for the aortic root as the response of the aortic root during stent deployment is dominated by the circumferential mechanical properties and as such is expected to capture the mechanical response of the aortic root correctly.[36] The effect of tissue calcifications on the residual stresses in the aortic root are not yet known and as a result were not included in our simulations.[34] Despite this, introduction of residual stresses may homogenize the stresses through the thickness of the aortic root,[20] resulting in increased vessel compliancy[34] and may increase the conformance of the artery to the stent and reduce stent eccentricity. An isotropic constitutive law, fitted to mechanical properties of pericardial leaflets in the circumferential direction, was used to model the glutaraldehyde fixed pericardial leaflets, based upon experimental studies that have suggested isotropic mechanical behavior[15,31] and also similar assumptions made in previous computational models.[1,35] The vector plot of the maximum principal strain directions (Figs. 5a and 5b) shows peak loading in the commissures in the circumferential direction, which supports the use of an isotropic model. However, it must be noted that the use of an isotropic material model may exacerbate peak stresses, as has previously been shown with anisotropic leaflet models predicting a more uniform stress distribution and reduced peak stresses.[1] Despite this simplification, the use of an isotropic model can still provide a model to compare the global structural response of the TAVR in asymmetric orifices. As the aortic wall thickness was much smaller than that of the circumferential and axial dimensions of the aortic root model, a plane stress analysis (shell elements) was deemed a valid assumption. In valve closure simulations the paravalvular skirt was considered as a rigid body and thus was not allowed to deform during leaflet closure. Introduction of a deformable valve skirt would allow for deflection of the leaflet commissures, which may reduce peak stresses in the leaflets similar to stent-tip deflection in previous bioprosthetic valve designs.[18] Peak stresses in our simulations may be exaggerated as a result of this modeling simplification. Leaflet opening was not simulated in our study, as peak stresses occur during valve closure, rather than at peak systole.[12] Finally, as clinical data on the effect of asymmetric TAVR on leaflet stresses and long term durability is not yet available, experimental validation of our simulations is not possible. Despite this however, the simulated stent deployment geometries had similar asymmetric geometries as those reported to occur *in vivo* (eccentricity = 0.68).[7,26] In addition to this, the final simulated closed leaflets showed the same closure characteristics

of an asymmetric TAVR in *in vitro* pulse duplicator studies, whereby incomplete leaflet apposition, regions that could allow for central leakage and buckling were also observed.[14]

Recent computational investigations of self expanding TAVRs have modeled stent expansion in idealized circular and realistic aortic root models.[22,33] In this study we developed the first computational model of a self expanding TAVR deployed in a realistic patient-specific aortic annulus, and we specifically modeled the TAVR leaflets to facilitate evaluation of the impact of Nitinol TAVR stent deployment geometry on leaflet mechanical behavior. Our results showed that peak stresses arising in the commissures of leaflets deployed in the realistic aortic root model were higher than those in a balloon-expandable Edwards Sapien valve characterized through a previous computational study (2.79 MPa vs. 2.16/2.32 MPa (Von Mises stress)).[2] The superior mechanical properties of the cobalt chromium stent and balloon expansion of the Edwards Sapien TAVR aided in forcing the asymmetric annulus to conform to the symmetric shape of the TAVR stent producing a circular orifice for the valve leaflets. The increased leaflet peak stresses in our model can be attributed to the asymmetric deployment of the Nitinol TAVR stent and the distorted leaflet geometry that was not captured in the circular Edwards Sapien TAVR. In addition to modeling the TAVR in circular and realistic patient-specific aortic root anatomy, we also developed models of the TAVR in idealized eccentric orifices, based on previous computational studies,[29] and to compare a single TAVR geometry under different deployment situations. While the results of the idealized eccentric morphology in the current study are within the range (1.1–2.2 MPa) of those reported previously,[29] the peak stresses were higher for the eccentric deployed TAVR ($e = 0.68$) compared to their model of the eccentric leaflet geometry (2.97 vs. 2.23 MPa).[29] However, it must be noted that the previous study[29] did not include the stent geometry, and was based on the eccentricity of Medtronic CoreValve, which in fact has been designed to ensure that the leaflets maintain circularity irrespective of asymmetric shape of the calcified annulus/native leaflets complex.[26] Thus the deployment eccentricity used in this study is correct for this specific stent design and provides a novel insight into tissue leaflet stresses arising in TAVRs under various deployment conditions.

Comparison of peak stresses recorded in the leaflets of the idealized eccentric and realistic valve models showed that peak stresses were higher in the idealized eccentric models. It must be noted however that the initial leaflet configuration differed for the idealized eccentric and realistic valve models, due to the leaflet attachment step. As a result the initial coaptation mismatch was more severe in the idealized eccentric models (Fig. 6b). Coaptation mismatch arises due to the free edge of one leaflet contacting the belly region of the opposing leaflet creating dominant leaflet(s) in the tri-leaflet arrangement (Fig. 6a). Bending of the dominant leaflets over the opposing leaflets during valve closure results in increased stresses in the commissure region of the non dominant leaflets. We propose that this phenomenon explains the increased commissural stresses in the idealized eccentric models compared to the leaflets in the realistic deployed TAVRs. We expect that leaflet buckling, as seen in the realistic models only, is a result of underexpansion of the TAVR stent from its nominal dimensions.[32] As a result, excess tissue relative to the stent orifice area caused buckling of the valve leaflets during closure.

Peak stresses in the aortic root (0.24 MPa) were located adjacent to the minor axis and were within the range experienced in previous studies (0.17–1 MPa).[2,6,34] It must be noted that different constitutive laws/material properties and a balloon expandable TAVR were used for those simulations.[2,6,34] Areas of stress concentrations were much lower adjacent to the major axis of the ellipse, indicating low exertion of stent radial force on this region of the annulus. In addition to this, incomplete stent apposition to the aortic root was found in this area which may be potential regions of paravalvular leak. In the TAVR stent, an asymmetric stress distribution was observed, with higher stresses recorded in the regions of the stent in contact with the minor axis of the ellipse compared to the direction of the major axis.

Patient-specific computational modeling of TAVR deployment can play a crucial role in the design, preoperative planning and prediction of post-operative TAVR performance.[2] In conjunction with patient-specific anatomies, finite element studies can be used to select the most appropriate valve sizing, minimizing the risk of valve under/over sizing and thereby reduce trauma to native leaflets and minimizing the occurrence of paravalvular leakage. Similar to Sun *et al.*,[29] we found that TAVR orientation in idealized valves played a role in minimizing peak stresses in the distorted leaflets. In our study however, modeling deployment of the TAVR in a realistic patient-specific aortic root allowed us to orientate the valve relative to the geometry of the aortic root. Our results show that preoperative planning of the orientation of TAVR within the aortic root may minimize the impact of potential stent distortion on leaflet function. Alignment of the commissures of the TAVR to those of native aortic root, reduced peak stresses from 2.97 MPa in the perpendicular configuration to 2.35 MPa in the commissure aligned configuration. In

circular valve deployment, the free edge of each leaflet contact the same region of the opposing leaflet creating organized coaptation lines. However in asymmetric deployment, as shown here, coaptation mismatch occurs creating a dominant leaflet(s) effect as shown in Fig. 6, thereby increasing the stresses in the commissural region of the non dominant leaflet(s). However it must be noted, that this behavior may be an artifact of the Finite Element Method, as the pressure boundary condition is applied normal to the leaflet surface. *In vivo*, flow reversal caused by pressure gradients across the valve leads to leaflet closure. Therefore the altered kinematics of the individual leaflets may be exacerbated and thus may overestimate the dominant leaflet effect that occurs. Despite the increase in peak stresses due to stent distortion in our realistic aortic root model, they did not exceed the ultimate tensile stress of bovine pericardium of 12.2 ± 3.5–17.7 ± 3.0 MPa.[30] However the increased stresses in the less dominant leaflets may result in accelerated progression of fatigue damage and may lead to leaflet tearing in the commissural region.[18] As a result, increased downward movement of the leaflet free edge may occur and the dominant leaflet effect will become more pronounced.[18]

CONCLUSION

In this study we developed finite element models of self expanding TAVR deployment in a realistic aortic root model to investigate the effect of TAVR stent asymmetry on leaflet kinematics and stress distribution. Our findings showed that, deployment of an idealized short profile TAVR stent lead to non-concentric deployment and irregular asymmetric leaflet morphology in a realistic aortic annulus model. TAVR deployed in a realistic aortic root resulted in increased peak loading in the commissural region of the TAVR leaflets compared to a TAVR under idealized circular deployment conditions. Furthermore orientation of the TAVR in the asymmetric aortic annulus, such that the commissures of the TAVR are aligned with the native valve commissures, minimized the effect of TAVR stent distortion on peak stresses in the TAVR leaflets. As the clinical use of TAVRs increase with the introduction of new valve technologies, imaging modalities and younger patient populations, the assessment and understanding of TAVR performance in asymmetric geometries is critical in the successful implantation of TAVR in patients with wide ranging aortic root morphologies. Computational modeling could be used in future applications to optimize the placement location, sizing and orientation of a TAVR and as a result increase leaflet durability, minimize paravalvular leakage and reduce coronary ostia obstruction. Based on the results of this study, we propose that in certain aortic root anatomies, preoperative planning of the orientation of the TAVR in the aortic root annulus might minimize stent and leaflet distortion and may thereby increase long term leaflet durability. In addition to this, our findings further the understanding of the impact of stent distortion on leaflet closing behavior and emphasize the requirement for optimization of TAVR designs to compensate for non-concentric deployment configurations *in vivo*.

ACKNOWLEDGMENTS

The authors acknowledge funding from the Engineering and Informatics Fellowship, National University of Ireland Galway, Science Foundation Ireland Short Term Travel Fellowship Award and the Irish Centre for High-End Computing (ICHEC).

DISCLOSURES

None.

REFERENCES

[1]Auricchio, F., M. Conti, A. Ferrara, S. Morganti, and A. Reali. Patient-specific simulation of a stentless aortic valve implant: the impact of fibres on leaflet performance. *Comput. Methods Biomech.* 17:277–285, 2012.

[2]Auricchio, F., M. Conti, S. Morganti, and A. Reali. Simulation of transcatheter aortic valve implantation: a patient-specific finite element approach. *Comput. Methods Biomech. Biomed. Engin.* 17:1347–1357, 2014.

[3]Auricchio, F., and R. L. Taylor. Shape-memory alloys: modeling and numerical simulations of the finite-strain superelastic behavior. *Comput. Methods Biomech.* 143:175–194, 1997.

[4]Auricchio, F., R. L. Taylor, and J. Lubliner. Shape-memory alloys: macromodeling and numerical simulations of the superelastic behavior. *Comput. Methods Biomech.* 146:281–312, 1997.

[5]Blanke, P., M. Russe, J. Leipsic, J. Reinöhl, U. Ebersberger, P. Suranyi, M. Siepe, G. Pache, M. Langer, and U. J. Schoepf. Conformational pulsatile changes of the aortic annulus: impact on prosthesis sizing by computed tomography for transcatheter aortic valve replacement. *J. Am. Coll. Cardiol. Interv.* 5:984–994, 2012.

[6]Capelli, C., G. Bosi, E. Cerri, J. Nordmeyer, T. Odenwald, P. Bonhoeffer, F. Migliavacca, A. Taylor, and S. Schievano. Patient-specific simulations of transcatheter aortic valve stent implantation. *Med. Biol. Eng. Comput.* 50:183–192, 2012.

[7]Cavero, M. A., J. Goicolea, C. García-Montero, and J. F. Oteo. Prognostic implications of asymmetric morphology in transcatheter aortic valve implantation: a case report. *Rev. Esp. Cardiol.* 65:104–105, 2012.

[8]Einstein, D. R., P. Reinhall, M. Nicosia, R. P. Cochran, and K. Kunzelman. Dynamic finite element implementa-

tion of nonlinear, anisotropic hyperelastic biological membranes. *Comput. Methods Biomech.* 6:33–44, 2003.
[9]Gunning, P., N. Saikrishnan, L. McNamara, and A. Yoganathan. An *in vitro* evaluation of the impact of eccentric deployment on transcatheter aortic valve hemodynamics. *Ann. Biomed. Eng.* 42:1195–1206, 2014.
[10]Hamdan, A., V. Guetta, E. Konen, O. Goitein, A. Segev, E. Raanani, D. Spiegelstein, I. Hay, E. Di Segni, M. Eldar, and E. Schwammenthal. Deformation dynamics and mechanical properties of the aortic annulus by 4-dimensional computed tomography insights into the functional anatomy of the aortic valve complex and implications for transcatheter aortic valve therapy. *J. Am. Coll. Cardiol.* 59:119–127, 2012.
[11]Iung, B., G. Baron, E. G. Butchart, F. Delahaye, C. Gohlke-Bärwolf, O. W. Levang, P. Tornos, J.-L. Vanoverschelde, F. Vermeer, E. Boersma, P. Ravaud, and A. Vahanian. A prospective survey of patients with valvular heart disease in Europe: The Euro Heart Survey on Valvular Heart Disease. *Eur. Heart J.* 24:1231–1243, 2003.
[12]Jermihov, P., L. Jia, M. Sacks, R. Gorman, J. Gorman, and K. Chandran. Effect of geometry on the leaflet stresses in simulated models of congenital bicuspid aortic valves. *Cardiovasc. Eng. Technol.* 2:48–56, 2011.
[13]Kleinstreuer, C., Z. Li, C. A. Basciano, S. Seelecke, and M. A. Farber. Computational mechanics of Nitinol stent grafts. *J. Biomech.* 41:2370–2378, 2008.
[14]Kuetting, M., A. Sedaghat, M. Utzenrath, J.-M. Sinning, C. Schmitz, J. Roggenkamp, N. Werner, T. Schmitz-Rode, and U. Steinseifer. *In vitro* assessment of the influence of aortic annulus ovality on the hydrodynamic performance of self-expanding transcatheter heart valve prostheses. *J. Biomech.* 47:957–965, 2014.
[15]Lee, J. M., S. A. Haberer, and D. R. Boughner. The bovine pericardial xenograft: I. Effect of fixation in aldehydes without constraint on the tensile viscoelastic properties of bovine pericardium. *J. Biomed. Mater. Res.* 23:457–475, 1989.
[16]Li, K., and W. Sun. Simulated thin pericardial bioprosthetic valve leaflet deformation under static pressure-only loading conditions: implications for percutaneous valves. *Ann. Biomed. Eng.* 38:2690–2701, 2010.
[17]Marlow, R. S. A general first-invariant hyperelastic constitutive model. In: Constitutive Models for Rubber III, edited by J. J. C. Busfield and A. H. Muhr. Lisse: Swets & Zeitlinger Publishers, 2003, pp. 157–160.
[18]Martin, C., and W. Sun. Simulation of long-term fatigue damage in bioprosthetic heart valves: effects of leaflet and stent elastic properties. *Biomech. Model. Mechanobiol.* 2013. doi:10.1007/s10237-013-0532-x.
[19]Padala, M., E. Sarin, P. Willis, V. Babaliaros, P. Block, R. Guyton, and V. Thourani. An engineering review of transcatheter aortic valve technologies. *Cardiovasc. Eng. Technol.* 1:77–87, 2010.
[20]Rachev, A., and S. E. Greenwald. Residual strains in conduit arteries. *J. Biomech.* 36:661–670, 2003.
[21]Rodes-Cabau, J. Transcatheter aortic valve implantation: current and future approaches. *Nat. Rev. Cardiol.* 9:15–29, 2012.
[22]Russ C., R. Hopf, S. Hirsch, S. Sundermann, V. Falk, G. Szekely, and M. Gessat. Simulation of transcatheter aortic valve implantation under consideration of leaflet calcification. In: Engineering in Medicine and Biology Society (EMBC), 2013 35th Annual International Conference of the IEEE, 2013, pp. 711–714.
[23]Sacks, M., and C. J. Chuong. Orthotropic mechanical properties of chemically treated bovine pericardium. *Ann. Biomed. Eng.* 26:892–902, 1998.
[24]Sacks, M. S., M. W. David, and D. E. Schmidt. On the biomechanics of heart valve function. *J. Biomech.* 42:1804–1824, 2009.
[25]Saikrishnan, N., S. Gupta, and A. P. Yoganathan. Hemodynamics of the Boston Scientific Lotus™ Valve: an *in vitro* study. *Cardiovasc. Eng. Technol.* 4(4):427–439, 2013.
[26]Schultz, C. J., A. Weustink, N. Piazza, A. Otten, N. Mollet, G. Krestin, R. J. van Geuns, P. de Feyter, P. W. J. Serruys, and P. de Jaegere. Geometry and degree of apposition of the CoreValve ReValving System with multislice computed tomography after implantation in patients with aortic stenosis. *J. Am. Coll. Cardiol.* 54:911–918, 2009.
[27]Smuts, A. N., D. C. Blaine, C. Scheffer, H. Weich, A. F. Doubell, and K. H. Dellimore. Application of finite element analysis to the design of tissue leaflets for a percutaneous aortic valve. *J. Mech. Behav. Biomed.* 4:85–98, 2011.
[28]Soncini, M., E. Votta, S. Zinicchino, V. Burrone, A. Mangini, M. Lemma, C. Antona, and A. Redaelli. Aortic root performance after valve sparing procedure: a comparative finite element analysis. *Med. Eng. Phys.* 31:234–243, 2009.
[29]Sun, W., K. Li, and E. Sirois. Simulated elliptical bioprosthetic valve deformation: implications for asymmetric transcatheter valve deployment. *J. Biomech.* 43:3085–3090, 2010.
[30]Sung, H.-W., Y. Chang, C.-T. Chiu, C.-N. Chen, and H.-C. Liang. Crosslinking characteristics and mechanical properties of a bovine pericardium fixed with a naturally occurring crosslinking agent. *J. Biomed. Mater. Res.* 47:116–126, 1999.
[31]Trowbridge, E. A., and C. E. Crofts. The extension rate independence of the hysteresis in glutaraldehyde-fixed bovine pericardium. *Biomaterials* 8:201–206, 1987.
[32]Tseng, E. E., A. Wisneski, A. N. Azadani, and L. Ge. Engineering perspective on transcatheter aortic valve implantation. *Int. Cardiol.* 5:53–70, 2013.
[33]Tzamtzis, S., J. Viquerat, J. Yap, M. J. Mullen, and G. Burriesci. Numerical analysis of the radial force produced by the Medtronic-CoreValve and Edwards-SAPIEN after transcatheter aortic valve implantation (TAVI). *Med. Eng. Phys.* 35:125–130, 2013.
[34]Wang, Q., E. Sirois, and W. Sun. Patient-specific modeling of biomechanical interaction in transcatheter aortic valve deployment. *J. Biomech.* 45:1965–1971, 2012.
[35]Xiong, F., W. Goetz, C. Chong, Y. Chua, S. Pfeifer, E. Wintermantel, and J. Yeo. Finite element investigation of stentless pericardial aortic valves: relevance of leaflet geometry. *Ann. Biomed. Eng.* 38:1908–1918, 2010.
[36]Zahedmanesh, H., D. John Kelly, and C. Lally. Simulation of a balloon expandable stent in a realistic coronary artery—determination of the optimum modeling strategy. *J. Biomech.* 43:2126–2132, 2010.
[37]Zegdi, R., V. Ciobotaru, N. Miléna, S. Ghassan, L. Antoine, L. Christian, D. Alain, and F. Jean-Noël. Is it reasonable to treat all calcified stenotic aortic valves with a valved stent?: results from a human anatomic study in adults. *J. Am. Coll. Cardiol.* 51:579–584, 2008.